Nanoscale

Cite this: *Nanoscale*, 2012, **4**, 511

www.rsc.org/nanoscale

PAPER

The properties of BiSb nanoribbons from first-principles calculations

H. Y. Lv,[a] H. J. Liu,*[a] X. J. Tan,[a] L. Pan,[a] Y. W. Wen,[a] J. Shi*[a] and X. F. Tang[b]

Received 26th October 2011, Accepted 28th October 2011
DOI: 10.1039/c1nr11585e

The structural, electronic and magnetic properties of BiSb nanoribbons (BSNRs) with different widths and edge configurations are investigated *via* the first-principles pseudopotential method. It is found that the pristine BSNRs with armchair edges (ABSNRs) are semiconductors and the band gaps exhibit a width dependent odd–even oscillation. In contrast, the pristine BSNRs with zigzag edges (ZBSNRs) are found to be metallic. When all the edge atoms are passivated by hydrogen, both the ABSNRs and ZBSNRs become semiconducting and the corresponding band gaps decrease monotonically with the increasing width. If, however, the edge atoms are partially passivated, the ABSNRs can be either semiconducting or metallic. Moreover, local magnetism appears when all the edge Sb atoms are passivated and there are one or more unsaturated Bi atoms. Using the nonequilibrium Green's function (NEGF) approach, we find that all the investigated odd-numbered ABSNRs have almost the same peak value of the power factor around the Fermi level. This is not the case for the even-numbered ABSNRs, where the peaks are twice that of when they are n-type doped. Our calculations indicate that BSNRs can have a very high room temperature figure of merit (ZT value), which makes them very promising candidates for thermoelectric applications.

1. Introduction

There is growing interest in the search for high performance thermoelectric materials, the efficiency of which is evaluated by the dimensionless figure of merit:

$$ZT = S^2GT/(\lambda_e + \lambda_p) \quad (1)$$

where S is the Seebeck coefficient, G is the electrical conductance, T is the absolute temperature, and λ_e and λ_p are the electronic and phonon thermal conductance, respectively. In order to compete with the conventional energy conversion method, the ZT value of a thermoelectric material should reach at least 3.0.[1] However, this goal hasn't been achieved experimentally so far. On the theoretical side, it is generally accepted that two- and one-dimensional nanostructures could have much larger ZT values compared with the bulk materials,[2,3] which has stimulated a lot of effort from the scientific community for about two decades.

Among many thermoelectric materials, Bi_2Te_3 has been intensively investigated due to its excellent thermoelectric performance around room temperature.[4–6] Teweldebrhan *et al.* reported the exfoliation of large-area crystalline films and ribbons from bulk Bi_2Te_3. The prepared quasi two-dimensional structures (with the thickness of a few atoms) were found to have high electrical conductivity and low thermal conductivity.[7,8] Coleman *et al.* proposed a general exfoliation technique to disperse a large range of layered compounds, including transition metal dichalcogenides, graphene, boron nitride (BN), and Bi_2Te_3.[9] Using such a simple method, the film and nanoribbon structures can be obtained in large quantities. Zahid *et al.* calculated the ZT value of the quintuple layer of Bi_2Te_3 and found that it could reach as high as 7.15.[10]

Bulk BiSb has a pseudo-layered structure similar to Bi_2Te_3; specifically, one Bi atom is connected to the three nearest Sb atoms, which forms a buckled honeycomb lattice. It is thus reasonable to expect that one could also obtain certain low-dimensional BiSb structures. Indeed, the BiSb nanowires,[11–14] nanotubes,[15] and thin films[16–18] have been successfully synthesized experimentally. In this work, we focus on another low-dimensional BiSb structure, namely, BiSb nanoribbons (BSNRs). Such kinds of structures are very similar to the well-known graphene nanoribbons,[19–21] but have quite different electronic and magnetic properties according to our first-principles calculations. Our results are also compared with those reported recently for Bi nanoribbons.[22] Moreover, the very favorable thermoelectric properties of the BSNRs are investigated *via* the nonequilibrium Green's function (NEGF) method.

2. Computational details

The structural, electronic and magnetic properties of BSNRs are calculated *via* a plane-wave pseudopotential formulation[23–25]

[a]*Key Laboratory of Artificial Micro- and Nano-structures of the Ministry of Education and School of Physics and Technology, Wuhan University, Wuhan, 430072, China. E-mail: phlhj@whu.edu.cn; jshi@whu.edu.cn; Fax: +86-27-68752569; Tel: +86-27-68754613*
[b]*State Key Laboratory of Advanced Technology for Materials Synthesis and Processing, Wuhan University of Technology, Wuhan, 430072, China*

within the framework of density functional theory (DFT). The code is implemented in the Vienna *ab initio* simulation package (VASP). The exchange–correlation energy is in the form of Perdew–Burke–Ernzerhof (PBE)[26] with a generalized gradient approximation (GGA). The geometry for each investigated BSNR is fully relaxed until the magnitude of the forces acting on all the atoms becomes less than 0.05 eV Å^{-1}. The **k** points are sampled on a uniform grid in the BSNR plane. We adopt a standard supercell geometry so that the BSNRs are aligned in an orthogonal array. The closest distance between each nanoribbon and its periodic image is set to be larger than 15 Å so that they can be treated as independent entities. The electronic transport properties of the BSNRs are calculated using the nonequilibrium Green's function (NEGF) approach[27–30] as implemented in the so-called Atomistix ToolKit code.

The phonon induced thermal conductivity (κ_p) of the nanoribbon can be expressed as:[31–33]

$$\kappa_p = \sum_{q,\lambda} \tau_{\lambda q} C_q(\omega_\lambda) v_{\lambda q}^2 \quad (2)$$

where $\tau_{\lambda q}$ and $v_{\lambda q}$ are, respectively, the relaxation time and group velocity of a phonon mode with the wave vector q and quantum number λ. $C_q(\omega_\lambda)$ is the specific heat per unit volume of each vibrational state with the angular frequency ω. According to the Matthiessen's rule, the total relaxation time can be expressed as a sum of the contributions from possible scattering mechanisms. In the present work, we only consider the scattering from the Umklapp process (τ_U) and the boundary (τ_B), so the phonon relaxation time τ_{ph} is given by:

$$\tau_{ph}^{-1} = \tau_U^{-1} + \tau_B^{-1} \quad (3)$$

In this formula, $\tau_B^{-1} = v_{\lambda q}/D$, where D is the size of the system. The second term can be written as $\tau_U^{-1} = \sum BT\omega_{\omega,q}^2 \exp(-\hbar\omega_m/k_B T)$, where B is a constant, T is the temperature and ω_m is the highest frequency of the phonon modes. As the cross-sectional area is not well defined for quasi-one-dimensional systems, such as BSNRs, we usually use the phonon induced thermal conductance (λ_p) instead of the thermal conductivity (κ_p) to calculate the ZT value.

3. Results and discussion

As mentioned previously, the BiSb mono-layer film may be exfoliated from the layered structure of bulk BiSb. According to our calculations, the energy per Bi–Sb atom pair of the mono-layer is only 0.24 eV higher than that of bulk BiSb, which suggests the energetic stability of the BiSb layer. The ABSNRs, or ZBSNRs, can be obtained by cutting the buckled BiSb layer along the armchair, or zigzag, direction. Following the notation for graphene nanoribbons,[21] the ABSNRs, or ZBSNRs, are classified by the number of dimer lines, or zigzag chains, across the ribbon width and are labeled as N-ABSNRs, or N-ZBSNRs. The initial structures of ABSNRs and ZBSNRs are illustrated in Fig. 1(a) and 1(d), respectively. We find that all the Bi–Sb bonds have the same length of 2.99 Å with bond angles of 91°. The buckling distance, Δ, denoted in Fig. 1(a) and 1(d) is 1.69 Å. Upon structure relaxations, we observe from Fig. 1(b) and 1(c) that the ABSNRs have obvious edge reconstructions and all the dangling bonds at the edges are eliminated. In the case of 9-ABSNR, the positions of the S1 and B1 atoms change a lot, which leads to the formation of additional B1–B2 and S1–S2 bonds. The corresponding bond length is 3.19 Å and 2.94 Å, respectively. Moreover, the distance between B2 and S0 is enlarged to 3.48 Å, which suggests the breaking of their covalent bond. The buckling distances are no longer uniform and are found to be 2.77 Å, 1.24 Å, 1.59 Å and 1.83 Å from the first to fourth dimer lines, respectively. Such edge reconstructions also lead to a slight change in the length of the original B2–S1, S1–B1, and B1–S2 bonds. Similar observations can be found for the 10-ABSNR, as shown in Fig. 1(c). The only difference is that for the odd-numbered ABSNRs, the reconstructed motifs at the two edges (B2–S1–B1–S2 and B8–S9–B9–S8) are symmetrically arranged; while for the even-numbered ABSNRs, they are only staggered. Such edge differences can give very different electronic properties, and we will come back to this point later. As for the ZBSNRs, the edge reconstructions are much smaller as indicated in Fig. 1(e) and 1(f). Indeed, we find that the bond angle only changes from 91° to 92° and the bond length from 2.99 Å to 2.96 Å. Besides this, there is no additional bond formed by structural relaxations for both the odd- and even-numbered ZBSNRs. The quite different edge configurations between the ABSNRs and the ZBSNRs will lead to their distinct electronic properties as discussed in the following paragraph.

Fig. 2 plots the total energies of the BiSb nanoribbons as a function of the ribbon width. We see that the ABSNRs are energetically more favorable than the ZBSNRs. This is consistent with the fact that there are obvious edge reconstructions in the ABSNRs compared with the ZBSNRs. The total energies of both systems decrease with the increasing ribbon width and finally approach the value of the BiSb buckled layer. This is an important piece of evidence for the stability of the BiSb nanoribbons. We have calculated the energy band structure of the BSNRs and found that all the ABSNRs are semiconductors while all the ZBSNRs are metallic. Detailed analysis of the band structures indicates that in the pristine ZBSNRs, the two unsaturated edge atoms with dangling bonds induce four energy bands crossing the Fermi level, which makes the system metallic. When the dangling bonds are eliminated by edge reconstruction (as observed in the ABSNRs) or by hydrogen passivation (discussed later), the system becomes semiconducting. Fig. 3 shows the calculated band gap of the ABSNRs as a function of the ribbon width (in terms of the number of dimer lines, N). We see that at small ribbon widths, the gaps of the even-numbered ABSNRs are relatively larger than those of the odd-numbered ones. A more interesting observation is that the gap exhibits an obvious width-dependent even–odd oscillation. Such behavior disappears gradually with increasing ribbon width, and finally the gap approaches that of the BiSb buckled layer. This picture is quite different from that found for graphene nanoribbons, where the energy gap shows three distinct family behaviors.[21] In order to explain such an oscillation, we plot in Fig. 4 the local density of states (LDOS) for the 9- and 10-ABSNR around the Fermi level. We see that the LDOS near the valence band maximum (VBM) have very similar shapes for the 9- and 10-ABSNR, while quite different LDOS are found near the conduction band minimum (CBM). We thus focus on the latter and the corresponding details are illustrated in the inset of Fig. 4. For the

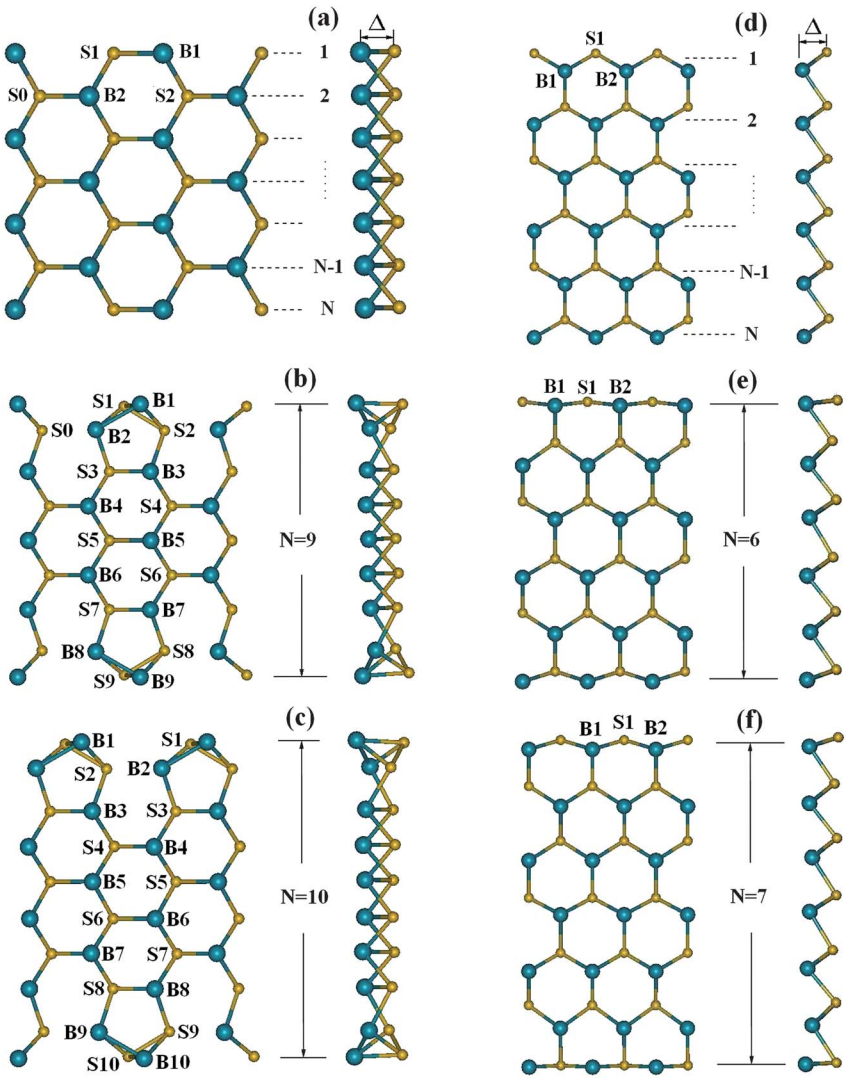

Fig. 1 Ball-and-stick model of the BSNRs: (a) the initial structure of an *N*-ABSNR, (b) the fully relaxed structure of 9-ABSNR, (c) the fully relaxed structure of 10-ABSNR, (d) the initial structure of an *N*-ZBSNR, (e) the fully relaxed structure of 6-ZBSNR, and (f) the fully relaxed structure of 7-ZBSNR. Note: B*k* ($k = 1, 2 \ldots 10$) and S*k* ($k = 0, 1, 2 \ldots 10$) represent different Bi and Sb atoms. Both the top and side views are shown.

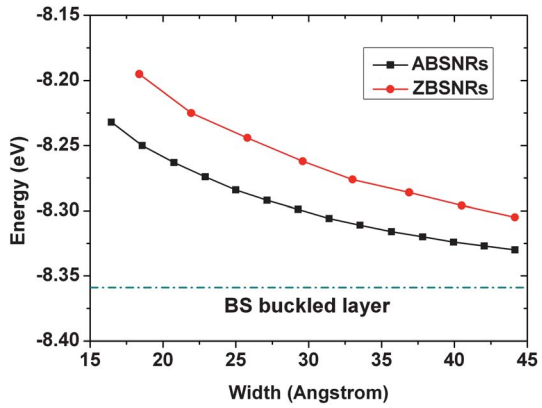

Fig. 2 The calculated total energies (in units of eV per Bi–Sb atom pair) of the ABSNRs and the ZBSNRs as a function of the ribbon width. The dotted line indicates the energy of the BiSb buckled layer.

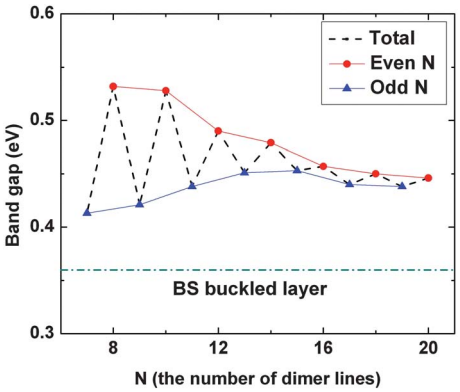

Fig. 3 The calculated band gap of the ABSNRs as a function of the ribbon width in terms of the number of dimer lines, *N*.

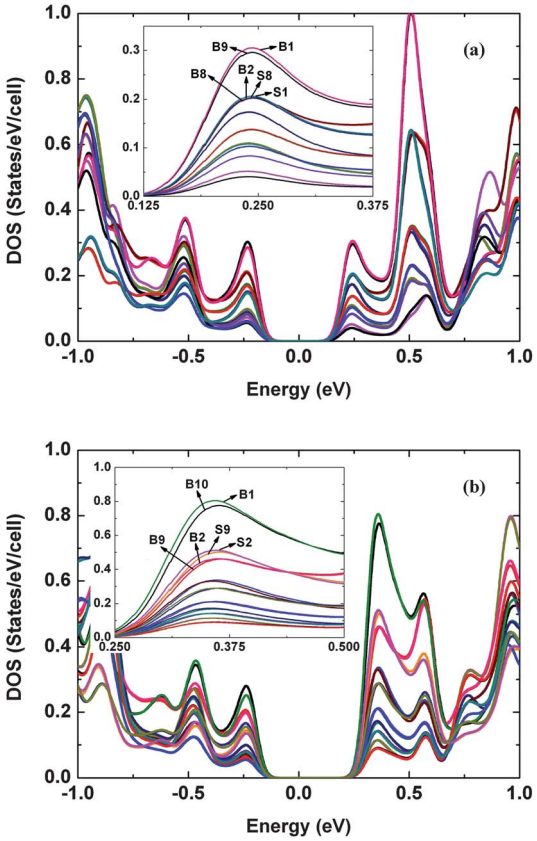

Fig. 4 The local density of states for the (a) 9-ABSNR and (b) 10-ABSNR. Inset is the enlarged parts around the CBM. Bk (k = 1, 2…10) and Sk (k = 1, 2…10) correspond to the atoms denoted in Fig. 1.

9-ABSNR, we see that the main contribution to the DOS comes from the B1 and B9 atoms, followed by the S1, S8, B2 and B8 atoms. There exists, however, a small difference for the 10-ABSNR. We see that the B1 and B10 atoms contribute to the DOS most, and then the S2 and S9 atoms, followed by the B2 and B9 atoms. If we focus on the positions of these atoms (see Fig. 1 (b) and 1(c)), we find that the atoms at the edges contribute to the DOS most and those close to the center less so. Since the edge atoms dominate the electronic states near the CBM, the different edge reconstructions of odd- and even-numbered ABSNRs may result in their different band gap behavior. In Fig. 5, we plot the band-decomposed charge densities of the VBM and CBM for the 9–11-ABSNRs. In the upper panel, we see that only one side of the nanoribbon contributes to the VBM. This suggests that the reconstructed atoms at the two edges have no interactions, which gives very similar valence bands for the 9–11-ABSNRs. However, we see from the lower panel of Fig. 5 that the two reconstructed motifs at the opposite edges contribute to the CBM at the same time. The interactions between them for the even-numbered ABSNRs are relatively stronger than those for the odd-numbered ones, which leads to the relatively larger band gaps of the former.[22,34] If the width of the ribbon is increased, the quantum confinement effect will dominate and the band gap decreases gradually.

We now consider the effect when the edge atoms of the BSNRs are passivated by hydrogen atoms. Unlike those observed in the

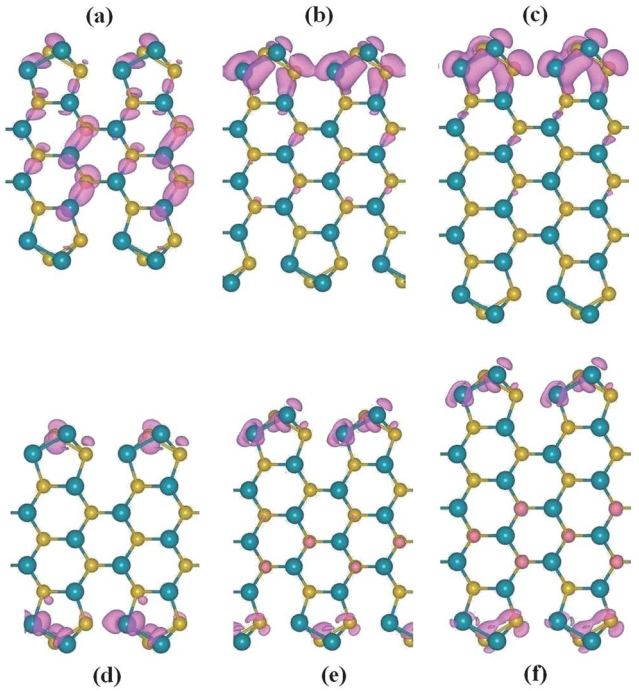

Fig. 5 The band-decomposed charge densities of the VBM for the (a) 9-ABSNR, (b) 10-ABSNR, (c) 11-ABSNR, and the CBM for the (d) 9-ABSNR, (e) 10-ABSNR and (f) 11-ABSNR.

pristine BSNRs, we find there are no edge reconstructions if all the edges are saturated. As shown in Fig. 6, both the ABSNRs and the ZBSNRs become semiconducting, and their band gaps decrease with an increasing ribbon width due to the quantum confinement effect. Moreover, the band gaps of the ABSNRs are generally larger than those of the ZBSNRs at the same ribbon width, and the difference becomes smaller when the ribbon width is increased. If, however, the edge atoms are partially passivated, we find a very different picture. In the unit cell of a pristine ABSNR, there are four edge atoms that have dangling bonds. If one edge atom is passivated, it can be either a Bi (denoted as 1H-B) or Sb (1H-S) atom. If two edge atoms are passivated, they can

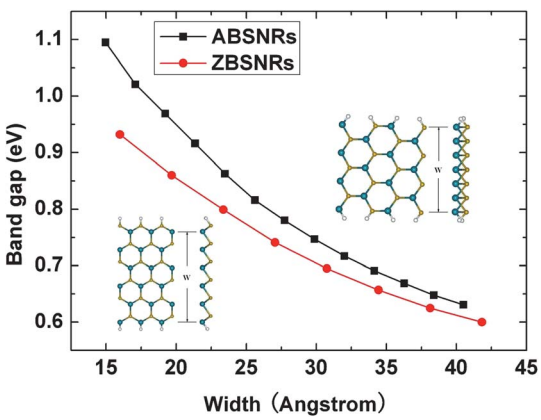

Fig. 6 The calculated band gaps for the hydrogen passivated ABSNRs and ZBSNRs as a function of the ribbon width. The insets are the fully relaxed structures of the ABSNR (upper right) and ZBSNR (lower left), where both the top and side views are shown.

be: (1) the Bi and Sb atoms on the same side (half H), (2) the Bi atom on one side with the Sb atom on the opposite side (2H-BS), (3) the Bi atom on one side with another Bi atom on the opposite side (2H-B), and (4) the Sb atom on one side with another Sb atom on the opposite side (2H-S). If three edge atoms are passivated, two possible configurations exist: (1) the Bi and Sb atoms on one side with another Bi atom on the opposite side (3H-B), and (2) the Bi and Sb atoms on one side with another Sb atom on the opposite side (3H-S). In total, there are eight different partially passivated products. Here, we take 7-ABSNR and 8-ABSNR as examples. The corresponding total energies, band gaps, and magnetic momentums are summarized in Table 1. We see that the partially passivated ABSNRs can be either metallic or semiconducting, depending on how the edge atoms are saturated. Our calculated results on the edge passivation (full or partial) demonstrate the possibility to tailor the electronic properties of the BiSb nanoribbons with fixed widths. It is worth mentioning that the sensitive dependence of the electronic properties on the edge passivation or non-covalent functionalization were also found in graphene nanoribbons.[35,36] Among the similar configurations, we see from Table 1 that 1H-S, 2H-S and 3H-S have relatively small energies, indicating that the Sb atom at the edge is energetically more favorable to be saturated with hydrogen. Moreover, it is interesting to note that for both the 7-ABSNR and 8-ABSNR, magnetism appears with the 2H-S and 3H-S configurations, where all the Sb atoms at the edges are passivated and there are one or more unsaturated Bi atoms. In order to find the origin of this magnetism we plot in Fig. 7 the iso-surface of the spin densities for the 2H-S and 3H-S configurations of 7-ABSNR and 8-ABSNR. Here, the areas inside, or outside, an iso-surface have larger, or smaller, densities. It can be clearly seen from the figure that for all the four cases we considered, the magnetism is mainly located at the unsaturated edge Bi atoms. It should be mentioned that if the edge atoms in the ZBSNRs are partially passivated by hydrogen atoms, all of them are found to be metallic and no magnetism appears. We must recognize that the experimental realization of a particular BSNR with partial passivation is still challenging. What we can expect from the theoretical calculations is that those configurations with the lowest energy could be possible products in experiments with different hydrogen concentrations.

We now move to the discussion of the thermoelectric properties. Here we take pristine ABSNRs as examples due to their favorable energies and interesting electronic properties. The

Table 1 The calculated total energies, E (in units of eV), band gaps, E_g (in units of eV), and magnetic momentum, M (in units of μB), of the 7- and 8-ABSNR with edge atoms partially passivated by hydrogen

	7-ABSNR			8-ABSNR		
Configuration	E	E_g	M	E	E_g	M
1H-B	−60.087	/	/	−68.569	/	/
1H-S	−60.427	/	/	−68.846	/	/
Half H	−63.754	0.72	/	−72.159	0.68	/
2H-BS	−63.211	/	/	−71.733	0.18	/
2H-B	−63.016	0.37	/	−71.191	/	/
2H-S	−63.527	0.095	0.12	−71.877	0.072	0.63
3H-B	−66.465	/	/	−74.870	/	/
3H-S	−66.807	0.025	0.44	−75.210	/	0.41

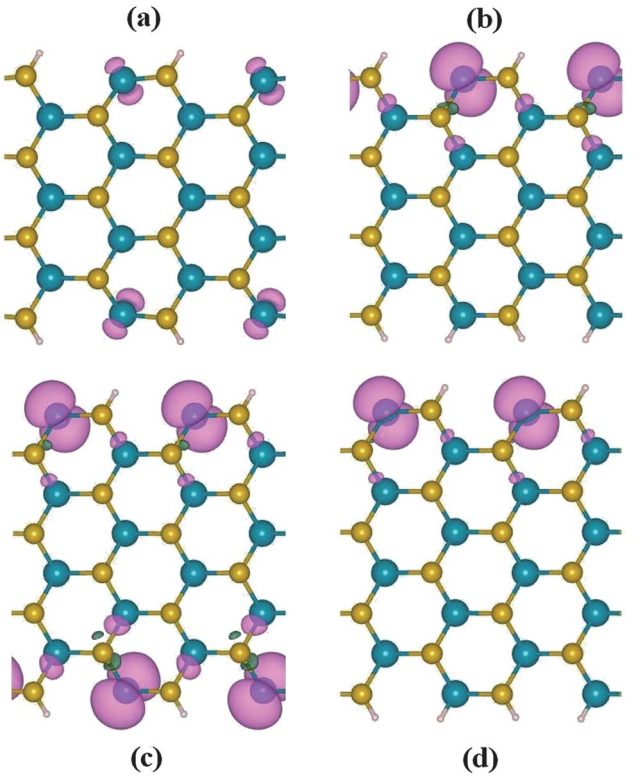

Fig. 7 The isosurfaces of the spin density for the partially passivated BiSb nanoribbons with different configurations: (a) 2H-S of 7-ABSNR, (b) 3H-S of 7-ABSNR, (c) 2H-S of 8-ABSNR, and (d) 3H-S of 8-ABSNR.

calculated electronic transport coefficients as a function of the chemical potential are plotted in Fig. 8 for the 7–12-ABSNRs. We see from Fig. 8(a) that the transmission near the VBM is almost the same for all the considered ABSNRs, which is consistent with their similar electronic structures mentioned above. This is, however, not the case near the CBM, where we find the even-numbered ABSNRs (8-, 10- and 12-ABSNR) have larger transmissions than the odd-numbered ones (7-, 9- and 11-ABSNRs). This observation suggests that the even-numbered ABSNRs may have better electronic transport properties when they are n-type doped. If we focus on the absolute value of the Seebeck coefficients shown in Fig. 8(b), we can see that the maximum values for the even-numbered ABSNRs are generally larger than those of the odd-numbered ones. Moreover, for the odd-numbered nanoribbons, the maximum Seebeck coefficients increase with the increasing widths. In contrast, all the even-numbered ABSNRs have similar peak values. Fig. 8(c) shows the corresponding electrical conductance as a function of the chemical potential. Near the Fermi level, the calculated electrical conductance for the odd-numbered ABSNRs decrease with the increasing ribbon widths, which is opposite to the tendency of the Seebeck coefficients. However, the electrical conductance values are nearly equal for all the even-numbered ones. The calculated power factors (PF = S^2G) are shown in Fig. 8(d), where we see that two main peaks appear around the Fermi level. For the odd-numbered ABSNRs, the opposing behavior of the Seebeck coefficient and the electrical conductance results in almost the

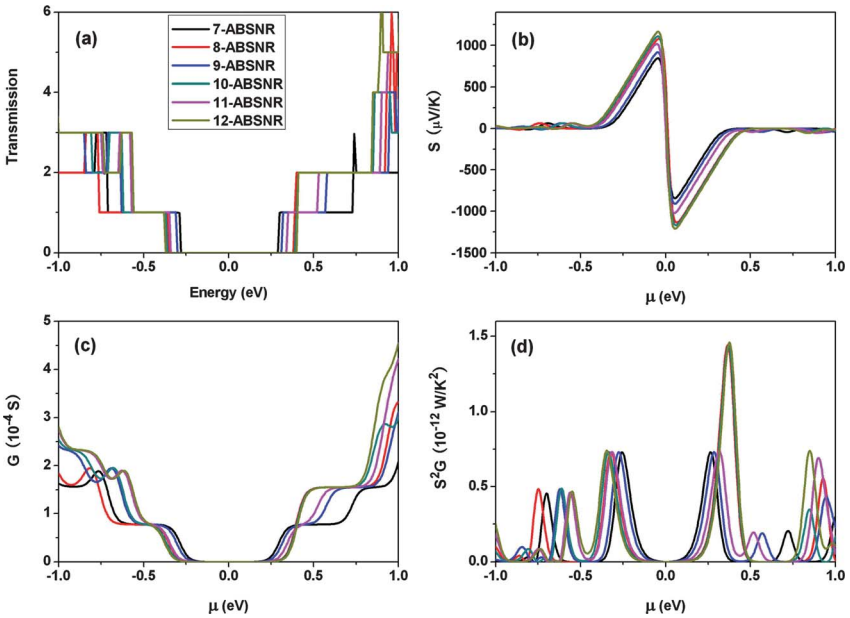

Fig. 8 The calculated transport coefficients for the 7–12-ABSNRs as a function of the chemical potential: (a) transmission function, (b) Seebeck coefficients, S, (c) electrical conductance, G, and (d) power factors, (PF = S^2G).

same peak values for both the p-type and n-type doping. As for the even-numbered ribbons, the peak value of the PF above the Fermi level is twice that below the Fermi level, which actually coincides with those of the odd-numbered ones.

To evaluate the figure of merit, we have calculated the phonon induced thermal conductance λ_p, which are found to be 0.018 and 0.012 nW K^{-1} for the 7-ABSNR and 8-ABSNR, respectively. Inserting these values into eqn (1), we can obtain the corresponding ZT values, as shown in Fig. 9. For the 7-ABSNR, the maximum ZT value is 5.2 for both the p-type ($\mu = -0.22$ eV) and n-type ($\mu = 0.23$ eV) doping. For the 8-ABSNR, the calculated ZT values are 6.6 and 9.2, for the p-type ($\mu = -0.28$ eV) and n-type ($\mu = 0.31$ eV) doping, respectively. These significantly larger ZT values suggest that, by proper doping,[37–39] the BSNRs could have very promising thermoelectric applications.

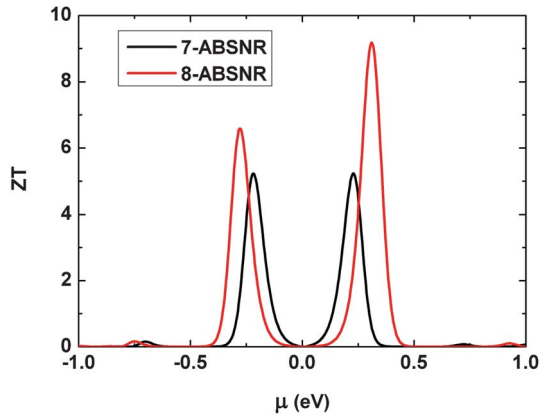

Fig. 9 The calculated ZT values for the 7-ABSNR and the 8-ABSNR as a function of the chemical potential.

4. Summary

In summary, our first-principles calculations indicate that the BiSb nanoribbons exhibit very rich electronic and magnetic properties, which are found to be closely related to their width and, particularly, the edge configurations (zigzag or armchair, pristine or passivated, *etc.*). Using the NEGF approach, the electronic transport properties of the nanoribbons have been calculated, which can be classified depending on whether the nanoribbon is even or odd numbered. In combination with the very low thermal conductance, much higher ZT values can be obtained. Our theoretical results suggest that BiSb nanoribbons could have potential applications in future nanoscale electronic devices, and may be excellent candidates for high-performance thermoelectric materials.

Acknowledgements

This work was supported by the "973 Program" of China (Grant No. 2007CB607501), the National Natural Science Foundation (Grant No. 51172167), and the Program for New Century Excellent Talents in University. We also acknowledge financial support from the interdiscipline and postgraduate programs under the "Fundamental Research Funds for the Central Universities". All the calculations were performed in the PC Cluster from the Sugon Company of China.

References

1 B. C. Sales, *Science*, 2002, **295**, 1248.
2 L. D. Hicks and M. S. Dresselhaus, *Phys. Rev. B: Condens. Matter*, 1993, **47**, 12727.
3 L. D. Hicks and M. S. Dresselhaus, *Phys. Rev. B: Condens. Matter*, 1993, **47**, 16631.
4 *CRC Handbook of Thermoelectrics*, ed. D. M. Rowe, CRC Press, Boca Raton, FL, 1995.
5 T. Tritt, *Science*, 1999, **283**, 804.

6 F. J. DiSalvo, *Science*, 1999, **285**, 703.
7 D. Teweldebrhan, V. Goyal, M. Rahman and A. A. Balandin, *Appl. Phys. Lett.*, 2010, **96**, 053107.
8 D. Teweldebrhan, V. Goyal and A. A. Balandin, *Nano Lett.*, 2010, **10**, 1209.
9 J. N. Coleman, *et al.*, *Science*, 2011, **331**, 568.
10 F. Zahid and R. Lake, *Appl. Phys. Lett.*, 2010, **97**, 212102.
11 Y.-M. Lin, S. B. Cronin, O. Rabin, J. Y. Ying and M. S. Dresselhaus, *Appl. Phys. Lett.*, 2001, **79**, 677.
12 Y.-M. Lin, O. Rabin, S. B. Cronin, J. Y. Ying and M. S. Dresselhaus, *Appl. Phys. Lett.*, 2002, **81**, 2403.
13 Y. Zhang, L. Li and G. H. Li, *Nanotechnology*, 2005, **16**, 2096.
14 X. C. Dou, G. H. Li and H. C. Lei, *Nano Lett.*, 2008, **8**, 1286.
15 X. C. Dou, G. H. Li, X. H. Huang and L. Li, *J. Phys. Chem. C*, 2008, **112**, 8167.
16 S. Cho, A. DiVenere, G. K. Wong, J. B. Ketterson and J. R. Meyer, *Phys. Rev. B: Condens. Matter*, 1999, **59**, 10691.
17 S. Cho, Y. Kim, A. DiVenere, G. K. L. Wong, J. B. Ketterson and J. R. Meyer, *J. Appl. Phys.*, 2000, **88**, 808.
18 M. Biçer, H. Köse and İ. Şişman, *J. Phys. Chem. C*, 2010, **114**, 8256.
19 Y.-W. Son, M. L. Cohen and S. G. Louie, *Nature*, 2006, **444**, 347.
20 D. A. Abanin, P. A. Lee and L. S. Levitov, *Phys. Rev. Lett.*, 2006, **96**, 176803.
21 Y.-W. Son, M. L. Cohen and S. G. Louie, *Phys. Rev. Lett.*, 2006, **97**, 216803.
22 L. Y. Zhu, T. T. Zhang and J. L. Wang, *J. Phys. Chem. C*, 2010, **114**, 19289.
23 G. Kresse and J. Hafner, *Phys. Rev. B: Condens. Matter*, 1993, **47**, 558.
24 G. Kresse and J. Hafner, *Phys. Rev. B: Condens. Matter*, 1994, **49**, 14251.
25 G. Kresse and J. Furthmüller, *Comput. Mater. Sci.*, 1996, **6**, 15.
26 J. P. Perdew, K. Burke and M. Ernzerhof, *Phys. Rev. Lett.*, 1996, **77**, 3865.
27 J. Taylor, H. Guo and J. Wang, *Phys. Rev. B: Condens. Matter Mater. Phys.*, 2001, **63**, 245407.
28 M. Brandbyge, J.-L. Mozos, P. Ordejón, J. Taylor and K. Stokbro, *Phys. Rev. B: Condens. Matter Mater. Phys.*, 2002, **65**, 165401.
29 H. Haug, and A.-P. Jauho, *Quantum Kinetics in Transport and Optics of Semiconductors*, Springer Solid State Series, Springer, Berlin, 2nd edn, 2008, vol. 123.
30 T. Markussen, A.-P. Jauho and M. Brandbyge, *Phys. Rev. B: Condens. Matter Mater. Phys.*, 2009, **79**, 035415.
31 S.-i. Tamura, Y. Tanaka and H. J. Maris, *Phys. Rev. B: Condens. Matter*, 1999, **60**, 2627.
32 J. X. Cao, X. H. Yan, Y. Xiao, Y. Tang and J. W. Ding, *Phys. Rev. B: Condens. Matter*, 2003, **67**, 045413.
33 J. X. Cao, X. H. Yan, Y. Xiao and J. W. Ding, *Phys. Rev. B: Condens. Matter Mater. Phys.*, 2004, **69**, 073407.
34 A. Streitwieser, *Molecular Orbital Theory for Organic Chemists*, Wiley, New York, 1961.
35 V. Barone, O. Hod and G. E. Scuseria, *Nano Lett.*, 2006, **6**, 2748.
36 A. Nduwimana and X.-Q. Wang, *ACS Nano*, 2009, **3**, 1995.
37 T. J. Scheidemantel, C. Ambrosch-Draxl, T. Thonhauser, J. V. Badding and J. O. Sofo, *Phys. Rev. B: Condens. Matter*, 2003, **68**, 125210.
38 G. K. H. Madsen, K. Schwarz, P. Blaha and D. J. Singh, *Phys. Rev. B: Condens. Matter*, 2003, **68**, 125212.
39 T. Thonhauser, T. J. Scheidemantel and J. O. Sofo, *Appl. Phys. Lett.*, 2004, **85**, 588.